J Nanopart Res (2015) 17:75
DOI 10.1007/s11051-014-2734-2

RESEARCH PAPER

Magnetic nanoparticles in medical nanorobotics

Sylvain Martel

Received: 19 August 2014 / Accepted: 4 November 2014 / Published online: 6 February 2015

Abstract Medical nanorobotics is a field of robotics that exploits the physics at the nanoscale to implement new functionalities in untethered robotic agents aimed for ultimate operations in constrained physiological environments of the human body. The implementation of such new functionalities is achieved by embedding specific nano-components in such robotic agents. Because magnetism has been and still widely used in medical nanorobotics, magnetic nanoparticles (MNP) in particular have shown to be well suited for this purpose. To date, although such magnetic nanoparticles play a critical role in medical nanorobotics, no literature has addressed specifically the use of MNP in medical nanorobotic agents. As such, this paper presents a short introductory tutorial and review of the use of magnetic nanoparticles in the field of medical nanorobotics with some of the related main functionalities that can be embedded in nanorobotic agents.

Guest Editors: Leonardo Ricotti, Arianna Menciassi

This article is part of the topical collection on Nanotechnology in Biorobotic Systems

S. Martel (✉)
NanoRobotics Laboratory, Department of Computer and Software Engineering, Institute of Biomedical Engineering, Polytechnique Montréal, Montréal, Canada
e-mail: sylvain.martel@polymtl.ca

Keywords Nanorobotics · Medical nanorobotic agents · Magnetic nanoparticles · Medical target interventions · Magnetic actuation · MRI · Local hyperthermia

Introduction

The main potential applications of medical nanorobotics include but are not limited to therapy such as target drug delivery, with other applications such as target diagnosis, and imaging. One of the benefices of using medical nanorobotic agents is their ability to target a precise location following controlled navigation along a pre-determined physiological path. For instance, using the shortest route, medical drug-loaded nanorobotic agents can avoid or at least minimize systemic circulation of highly toxic therapeutics that affect healthy tissues and organs, while increasing the therapeutic efficacy for a given injected dose of therapeutics.

Unlike larger robotic agents that are most often dedicated to surgical tasks, most medical interventions involving nanorobotic agents will use them a single time without the possibility or the willingness for recovery. This is the case for most nanorobotic agents including the ones aimed at delivering therapeutics to a tumor. As such, medical nanorobotic agents must be made of biodegradable materials and the embedded components must be sufficiently small to be later eliminated from the body. This is typically the case for

the magnetic materials embedded in medical nanorobotic agents that will generally be in the form of magnetic nanoparticles (MNP). As such, the use of a permanent magnet that is often embedded in larger untethered medical robots aimed at operating in wider physiological spaces and which can be recovered after the intervention is generally not an option for the implementation of medical nanorobotic agents. Indeed, not retaining their magnetization state can prove to be especially important for avoiding an aggregation of several nanorobotic agents or a cluster of MNP following a biodegradation of the nanorobotic agents that will retain the form of a relatively large entity once the patient is no longer exposed to a magnetic field following the completion of the medical intervention.

In this respect, the type and the characteristics of magnetic materials that constitute each MNP become critical choices. The classification of a material's magnetic properties is based on its magnetic susceptibility (χ) which is particularly important for magnetic pulling-based actuation methods used during navigation in larger vasculatures or physiological spaces, and for MRI-based tracking during such closed-loop navigation phase, as well as for MR-imaging of the larger artifacts created by such agents to assess the targeting efficacy of these nanorobotic agents following the navigation phase since their overall sizes are generally well below the spatial resolution of all medical imaging modalities. The magnetic susceptibility is defined by the ratio of the induced magnetization (M) to the applied magnetic field (H).

Based on the alignment and response of magnetic dipoles, materials have been classified as diamagnetic, paramagnetic, ferromagnetic, ferrimagnetic, and antiferromagnetic as schematically illustrated in Fig. 1.

Although diamagnetic materials do not retain magnetic properties when the external magnetic field is removed, the magnetic moment which is antiparallel to H results in negative and negligible susceptibility levels (-10^{-6} to -10^{-3}). On the contrary, paramagnetic materials such as ferrimagnetic and ferromagnetic materials have magnetic moments parallel to H with susceptibilities in the order of 10^{-6} to 10^{-1}. For instance, ferrimagnetic properties occur in an oxide of iron known as magnetite (Fe_3O_4) which is an interesting fact in medical nanorobotic applications considering that such a material in the form of MNP is widely used as a contrast agent in clinical Magnetic

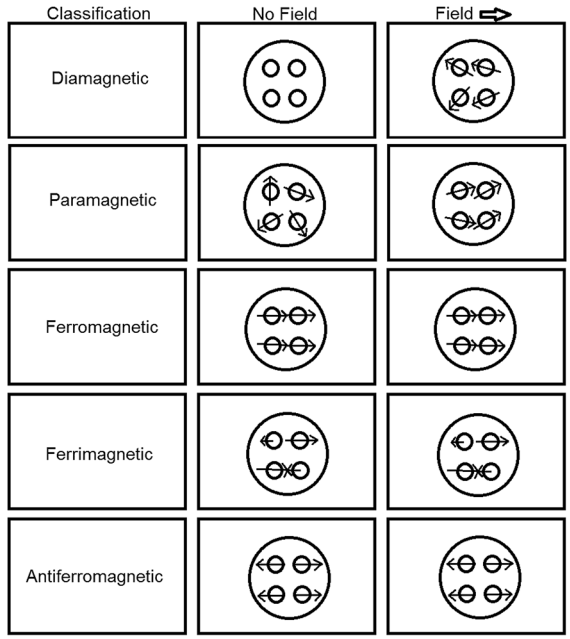

Fig. 1 Basic schematics illustrating the alignment of the magnetic dipoles of various types of magnetic nanoparticles inside a nanorobotic agent

Resonance Imaging (MRI). Iron oxide magnetite (Fe_3O_4) and its oxidized form maghemite (γ-Fe_2O_3) in particular are used extensively due to their low toxicity and their known pathways of metabolism, making these materials attractive for nanorobotic agents designed for medical applications. In medical nanorobotics, Fe_3O_4 MNPs are generally preferred to γ-Fe_2O_3 MNP due to its higher saturation magnetization. The magnetization state for a ferrimagnetic material is the result of the alignment of microscopic regions in the material known as magnetic domains or magnetic moments. In a ferrimagnetic material, neighboring magnetic moments have opposite orderings that would cancel out the overall magnetic field of the material except that a magnetic field still results due to small differences between neighboring magnetic domains. For ferromagnetic materials such as iron, nickel, and cobalt, the magnetic moments align in the same direction and parallel to each other to produce a larger magnetization state, allowing higher directional pulling forces to be induced on the nanorobotic agents during the navigation phase toward the target physiological regions.

In the form of a MNP with an overall size in the order of up to tens of nanometers, ferrimagnetic or ferromagnetic materials become a single magnetic

domain resulting in a relatively large magnetic moment. For instance, the domain size of Fe_3O_4 is 15-80 nm (Hergt et al. 2008). However, above a specific temperature level known as the blocking temperature (T_B), the thermal energy becomes sufficient to induce free rotation of the MNP resulting in a loss of the net magnetization when not being exposed to an external magnetic field H. This lack of remnant magnetization (Mr in Fig. 2) after removal of an external magnetic field is the main characteristic of a superparamagnetic MNP. The typical magnetization curve of a superparamagnetic MNP compared to a ferromagnetic particle is depicted in Fig. 2.

Such superparamagnetic property enables the MNP to maintain their colloidal stability (i.e., remain dispersed in a liquid medium for long periods of time) and to avoid aggregations following the targeting phase once the patient is removed from the magnetic field, hence allowing their use in clinical targeting interventions. But for medical nanorobotics, because superparamagnetic MNP leads to a reduction of the saturation magnetization (M_S), the actuation forces being induced on navigable agents will be decreased. Although this decrease can be somewhat compensated by increasing the number of MNP embedded in each agent, it already shows the challenges such as selecting the appropriate size of the magnetic particles for implementing multifunctional nanorobotic agents within the constraints imposed by clinical interventions.

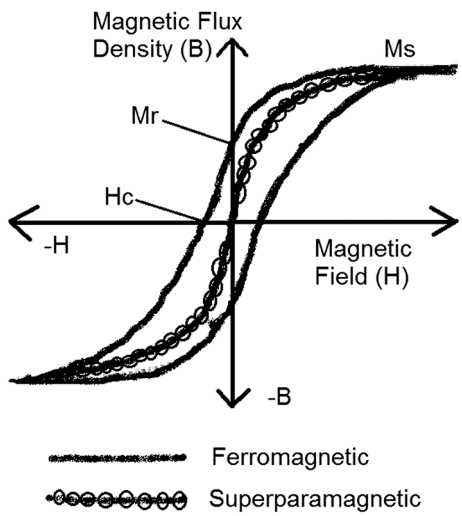

Fig. 2 Magnetization curve for a superparamagnetic MNP showing no hysteresis and hence no residual magnetization and coercivity compared to a ferromagnetic particle

The range of magnetic particles' sizes that can be considered in medical nanorobotics can be categorized as multi-domain (MD), pseudo-single-domain (PSD), single-domain (SD), and superparamagnetic (SPM). The maximum coercivity for a given magnetic material occurs within its SD range. Higher coercivity (Hc in Fig. 2 being the resistance of a magnetic material to becoming demagnetized), for instance, is required to enhance hyperthermia through hysteresis losses as discussed later in this paper. The magnetization curve of a SD material will then resemble the one depicted in Fig. 2 for the MD ferromagnetic material but rotated clockwise and with a larger Hc and a lower M_S. Indeed, particles in the MD range would lead to a larger saturation magnetization for enhanced actuation and higher MR-image artifacts to ease achieving higher real-time MR-tracking of navigable agents during travel. But MD particles can typically only be considered for clinical applications if such agents can be recovered, which is not possible in many interventions where medical nanorobotics would perform better than with larger untethered robots. In the PSD range, small MD grains exhibit a mixture of SD-like (high remanence) and MD-like (low coercivity) characteristics. SD particles have also a higher remanence that MD which may not be suitable in particular medical interventions such as in drug deliveries in cancer therapy. But as the particle size continues to decrease within the SD range, another critical threshold is reached at which both remanence and coercivity reach zero, and it is referred to as the superparamagnetic range. In an applied field, there will be a net statistical alignment of magnetic moments analogous to paramagnetic particles except that the magnetic moment is not that of a single atom but to an SD particle containing a range of approximately 10^5 atoms. Hence, a superparamagnetic MNP would have a much higher susceptibility value than that for simple paramagnetic particle which is highly desirable in the context of medical nanorobotics. For spherical MNP, the transition from superparamagnetic to SD can be determined by the following equation:

$$r_0 = (6k_B T_B / K)^{1/3}, \quad (1)$$

where r_0 is the transition point from superparamagnetic to SD, with k_B, T_B, and K being the Boltzmann constant, the blocking temperature, and the anisotropy constant, respectively. Table 1 provides approximate (since several variables can influence sensibly these

Table 1 MNP diameters (approx.) for transition from superparamagnetic to single-domain regimes

Materials	Superparamagnetic MNP Diameter (nm)	Single Domain MNP Diameter (nm)
CoPt	<2	2–58
FePt	<3	3–55
Co	<10	10–80
$CoFe_2O_4$	<10	10–100
FeCo	<20	20–50
Fe_3O_4	<25	25–85
Ni	<30	30–85
Fe_2O_3	<30	30–90

values such as a change in temperature for operations in the human body) MNP diameters for transition from superparamagnetic to SD regimes from the smallest to the largest diameters for some of the main MNP materials.

Actuation

Actuation or the capability of such untethered nanorobotic agents to move toward a physiological targeted site is critical for the success of the intervention. Magnetic-based actuation in medical nanorobotics can be categorized as pulling-based, torque-based, and magnetically guided self-propelled actuation methods. Especially for pulling-based actuation approaches, the saturation magnetization (M_S) value corresponding to the complete alignment of all individual moments becomes smaller in MNP compared to the corresponding saturation magnetization value obtained in bulk form due mainly to disordered crystal structure resulting from high surface curvature which increases with a reduction of the overall size of the particle.

For example, M_S values for magnetite MNP will typically be in the range of 30–50emu/g compared to approximately 90emu/g in bulk forms (Gupta and Gupta 2005). Indeed, bulk materials have constant physical properties regardless of their sizes but at the nanoscale, size-dependent properties are often observed. Saturation magnetization at such levels can be typically achieved by exposing the MNP to a magnetic field of approximately 1.5 T and higher as depicted in Fig. 3.

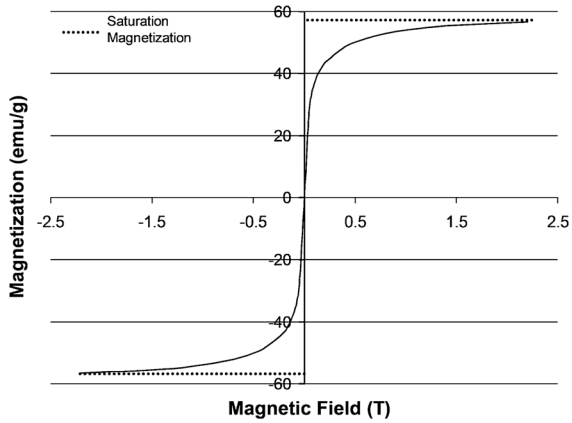

Fig. 3 Typical magnetization curve of Fe_3O_4 magnetic suspensions (Mathieu and Martel 2009)

With an external magnet or electromagnet, the field strength decays rapidly with distance. For instance, the maximum field strength achievable for whole body interventions with existing magnetic actuation platforms based on a permanent magnet or a configuration of electromagnetic coils is approximately 0.1 T. From the magnetization curve in Fig. 3 for instance, it can be observed that the magnetization level of the MNP at 0.1 T will be much lower than M_S resulting in a much lower induced directional pulling force on the MNP from a given magnetic gradient and hence, on the medical nanorobotic agents as well.

By immersing the patient in a uniform magnetic field of 1.5 T or more such as in the tunnel of a clinical MRI scanner (typical B_0 of 1.5 or 3T in more recent systems), saturation magnetization for such MNP can be achieved for whole body interventions allowing maximum effective gradient-based directional pulling forces anywhere within the body. Such 3D gradients can be produced by the scanner's imaging coils resulting in body depth-independent induced forces on the nanorobotic agents. This is the fundamental principle of an approach known as magnetic resonance navigation (MRN) (Mathieu et al. 2006, 2007). With such an approach, the directional induction force can be computed from Eq. 2 where $M = M_S$ and V_M represents the effective or total volume of all MNP embedded in each nanorobotic agent.

$$\vec{F} = V_M\left(\vec{M} \cdot \nabla\right)\vec{B}, \tag{2}$$

where

$$\nabla = \left[\frac{\partial}{\partial x} \quad \frac{\partial}{\partial y} \quad \frac{\partial}{\partial z}\right]^T. \tag{3}$$

Metallic MNP made of materials such as nickel, iron, and/or cobalt, etc., although not as chemically stable as iron oxide MNP, can potentially be embedded in medical nanorobotic agents where higher magnetization saturation levels compared to Fe_3O_4 MNP are required. Because of the formation of oxides when exposed to water and oxygen, these MNP are typically protected with a thin layer of coating made of materials such as dextran, gold, silica, or graphite, to name but a few examples. Such coating avoids a decrease of M_S by oxidation, and the release of metallic ions. Combining different metallic materials within the same MNP can also increase the saturation magnetization level of the MNP. For example, Cobalt (Co), iron (Fe), and FeCo nanoparticles exhibit a M_S around 140, 180, and 220emu/g, respectively (Pouponneau et al. 2012). Indeed, FeCo nanoparticles are receiving increased attention because of the extremely high M_S values (Reiss and Hutten 2005) which make them highly suitable (independently of biocompatibility issues) for medical nanorobotic agents for increasing the induced pulling force, in some cases by lowering the amount of embedded magnetic material to allow more room for the therapeutic payload, or to decrease the amount of MNP injected in the body, and/or to achieve further miniaturization of the nanorobotic agents.

Despite the relatively high saturation magnetization levels, many MNP must be embedded in each nanorobotic agent to increase the magnetic induction volume which is highly insufficient using distributed (monodispersed or polydispersed) MNP flowing independently in the vascular network, for example. For instance, preliminary investigations of the hydrodynamics of drug targeting suggest that for a magnetite-based MNP exposed to a magnetic flux density of 0.2 T would require field gradients of approximately 8T/m in the femoral arteries and greater than 100T/m in carotid arteries (Voltairas et al. 2002). Unless the target is extremely close to the magnetic source which is generally not the case especially when operating deeper in the tissue, such high gradients cannot be generated in the context of medical nanorobotics. As such, increasing the magnetic induction volume by embedding a sufficiently large quantity of MNP in each nanorobotic agent becomes mandatory in order to decrease the amplitude of the switching directional gradients within technological and physiological limits. Indeed, unlike conventional magnetic drug targeting (MDT) approaches which rely on a constant unidirectional gradient generally produced by a single permanent or electromagnet placed near the target, magnetic pulling forces induced on medical nanorobotic agents rely on 3D directional gradients to allow navigation prior to reach the target. For whole body interventions, the present technological limitation for sufficiently fast directionally changed gradients for clinical applications using nanorobotic agents is in the order of 300–400mT/m (Martel 2014).

Increasing the magnetic induction volume has been done for the synthesis of the first therapeutic nanorobotic agent known as Therapeutic Magnetic Micro-Carrier (TMMC) (Pouponneau et al. 2011, 2014). To provide an example, $>$ 300 mT/min a $B_0 = 1.5$T was required to influence sufficiently the path of such nanorobotic agents to target pre-determined lobes in the liver of rabbit models after a transition through the hepatic artery. These TMMC (also referred to as Magnetic Drug Eluting Beads (MDEB) when used for liver chemo-embolization) carried a therapeutic payload consisting of 3.2 ± 0.5 % doxorubicin (DOX) and were synthesized with 37 ± 2.7 % (w/w) FeCo MNP ($\text{Ø} = 206 \pm 62$ nm, $M_S = 202 \pm 6$emu/g) coated with a few nanometer thick graphite shell embedded in a spherical biodegradable polymer (poly(lactic-co-glycolic acid) -PLGA) matrix ($\text{Ø} = 53 \pm 19$ μm) resulting for the whole TMMC to a $M_S = 72 \pm 3$emu/g. The larger diameter of the FeCo MNP made of a few magnetic domains aimed at increasing the local inhomogeneity of the B_0 field to ease the detection and localization of the TMMC by MRI.

Initial versions of the TMMC had tightly mechanically (structurally by the polymer matrix) coupled MNP being distributed randomly within the biodegradable polymer matrix. Such a configuration results in a demagnetization factor of 1/3 due to the spherical shape of each non-interacting (no dipolar interaction) distributed MNP. Such demagnetization factor is the result of free magnetic dipoles induced on both ends of the magnetized MNP, giving rise to a magnetic field referred to as the demagnetization field in the opposite direction to the magnetization of the MNP. This fact suggests that the overall magnetization could be enhanced by embedding the MNP in chain-like configurations resulting in a much lower

demagnetization factor. But when such MNP are aligned in a chain or needle-like fashion, the hysteresis loop is affected and the magnetic parameters such as remanence and coercivity notably increase, which may be taken into account for some particular nanorobotic target medical interventions. These changes in the magnetic properties are related to the demagnetization factor and to the orientation of the magnetic moments of the MNP along one of the easy magnetization axes (Ngo and Pileni 2000).

Furthermore, initial experimental results conducted in animal models suggest that magnetic biodegradable pulling-based nanorobotic agents such as the TMMC should be made as large as possible for embolization but small enough to navigate beyond the arterial network. As such, nanorobotic agents with diameters between approximately 150 and 300 μm (approx. 50 μm in smaller animal models such as rabbits) would allow navigation and an embolization in the human arterioles where the drug could be released, hence preventing such agents to bypass the arterioles and to re-circulate unintentionally in the systemic vascular network due to insufficient magnetic induction volume and magnetization to retain the nanorobotic agents at the drug release site for a sufficient amount of time required for completing the release of the drug. Such increase in the overall volume would also increase the magnetic induction volume per nanorobotic agent, yielding larger induced pulling directional forces.

But unlike for larger (diameter in the millimeter range) agents, the induced force on such microscale nanorobotic agents can be made sufficient only for steering purpose. Intra-arterial injections are typically used since the blood flow in arteries generally goes toward physiological targets in medical nanorobotics such as in cancer therapy where arteries carry oxygen and nutrient toward the tumoral lesions. Such blood flow is typically exploited to provide the propelling force to the nanorobotic agents being steered by directional magnetic gradients. Because of the excessive arterial blood flow (e.g., in the order of 0.3 m/s), not enough time is allowed in most cases for such gradients to deviate sufficiently such nanorobotic agents toward the appropriate branch at each vessel's bifurcation that leads to the pre-determined target region. One logical approach to solve this issue is to decrease the blood flow appropriately through the use of a balloon catheter or other potential devices that ideally could be synchronized with the MR-navigation sequences (Martel 2013a). This can be done at the expense of extending the time of the interventions. This may become an issue particularly with the delivery of a large therapeutic dose. Indeed, since MRN is acting on all nanorobotic agents simultaneously, a number of consecutive injections of boluses of nanorobotic agents totalizing the dose that needs to be delivered would be required. The size of these boluses typically becomes smaller when targeting deeper regions being accessed through the vascular network since the lengths of the branching vessels tend to become shorter after each vessel's bifurcation. Such boluses can take the form of independent agents or as aggregates of nanorobotic agents. The formation of aggregates results into a significant increase of the magnetic induction volume. Due to dipole–dipole interactions (dipolar coupling) between the nanorobotic agents, ellipsoidal (prolate) or chain-like aggregations can form with the easy (longitudinal) axis being parallel to the B_0 field during MRN which can lead to potential unwanted embolizations if the dipole–dipole interactive force between neighborhood agents is too high, especially when the navigation path becomes more perpendicular to the B_0 field. Ideally for optimal results achieved within the shortest possible intervention time, the dipole–dipole interactive force must be adjusted during the synthesis of the nanorobotic agents (by modifying the density of MNP, by modifying the coating of the MNP or the agent itself, etc.) with regard to the required aggregate's breaking force that can be provided by the blood flow and other factors such as the shear stress forces for instance when closer to a vessel's wall. The determination of such an optimal range of dipole–dipole interactive forces would require an a priori knowledge of the blood velocity that will be used and other parameters such as the angles of each segment in the navigation path with regard to the *Bo* field, and the diameter of the blood vessels. As such, the development of models (Belharet et al. 2013) to predict the behavior of such nanorobotic agents based on the characteristics of the MNP and the agents taken from physiological measurements gathered prior to the target interventions may prove to be a suitable tool to help achieving maximum targeting efficacy for each particular intervention.

The standard interventional method based on magnetic pulling for navigating nanorobotic agents

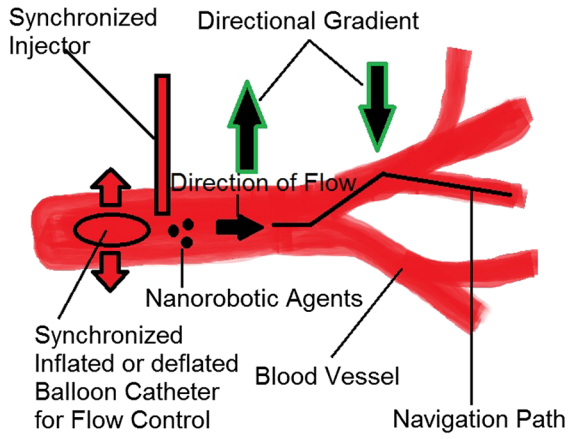

Fig. 4 Basic schematic illustrating the typical interventional pulling-based method

is described in the simplified schematic depicted in Fig. 4. The blood flow rate in the artery is controlled through an inflating–deflating balloon catheter (or similar device). The latter is synchronized with the injector which in its present version consists of several small coil wounds positioned at regular intervals around a silicon tube. By synchronizing the current flow with the injection flow, it is possible to capture and to release the nanorobotic agents in a periodic fashion. The detection system in the injector exploits the change in voltage between two coupled resonant inductance-capacitance (LC) resonance circuits installed at the tip of the injector, when a bolus of nanorobotic agents exits the injector. Such detection triggers a signal to synchronize the magnetic navigation sequence. If a synchronized MR-tracking sequence is initiated during the navigation phase, the blood flow is modulated according to the time of the tracking sequence using the synchronized balloon catheter while the injection sequences are being modified. Such tight communication link between the various sub-systems is essential to ensure proper optimized operations.

Once injected, directional gradients are then applied to direct the nanorobotic agents toward the appropriated branching vessel with the blood flow being adjusted to allow sufficient time for the gradients to deviate the agents along the planned path. At this step, nanorobotic agents can navigate independently or the formation of aggregates may be selected to increase the effective magnetic volume and hence the total directional force being induced. By using the blood flow for displacement, the opposite hydrodynamic drag force (Eq. 4) that could break such aggregates becomes negligible since $\boldsymbol{v}$ being the motion of the nanorobotic aggregates relative to the fluid flow is typically null.

$$\vec{F}_D = -\frac{1}{2}\rho_f A C_d \cdot \|\vec{v}\| \, v \tag{4}$$

In Eq. 4, ρ_f is the fluid density with A being the nanorobotic agent or the aggregate's hydrodynamic reference area. C_d is defined as a dimensionless drag coefficient related to the Reynolds number Re. When a directional force is induced according to Eq. 2 to steer (pull) the aggregate toward the desired branching vessel, $\boldsymbol{v} \neq 0$ and therefore, the resulted drag force (Eq. 4) would have to be smaller than the dipolar field retaining the nanorobotic agents together. For two neighborhood nanorobotic agents, such magnetic dipole–dipole interaction energy can be estimated as

$$E_D = -\frac{\mu_0}{4\pi}\left(\frac{3\,(\vec{\mu}_A \cdot \vec{r}_{AB})(\vec{\mu}_B \cdot \vec{r}_{AB})}{\vec{r}_{AB}^{\,5}} - \frac{\vec{\mu}_A \cdot \vec{\mu}_B}{\vec{r}_{AB}^{\,3}}\right); \quad where\ \vec{r}_{AB} = \|\vec{r}_{AB}\| \tag{5}$$

In Eq. 5, μ_0 is the permeability of vacuum, with μ_A and μ_B being a point-like dipole located at the center of spherical MNP or agents designed A and B, respectively, with the vector r_{AB} joining the center of the two dipoles. Accordingly, the lowest energy configuration would correspond to the two magnetic moments aligned head-to-tail, forming with many agents, an aggregate with the long (easy) axis oriented parallel to the B_0 field. As such, the variable A in Eq. 4 of the corresponding aggregate will vary during the steering phase according to the angle between the easy axis of the aggregate and the direction of the magnetic gradient being applied for navigation purpose. In other words, the directions of the programmed navigation path have to be taken into account in determining the minimum dipolar interactive force required during the synthesis of the nanorobotic agents. Such dipolar interactive force must also be able to sustain other forces related to the vessel walls in the context of wall retarding effects and/or shear-stress forces for instance when closer to a vessel's wall.

Although the above information can be used to determine the minimum dipole–dipole interactive force between the MNP-based nanorobotic agents,

such dipole–dipole force must be lower than an achievable breaking force. Failing to synthesize the MNP-based agents with a dipole–dipole interactive force below such achievable breaking force would yield unpredicted embolization that may not only be suitable in a medical point-of-view, but also will prevent such nanorobotics agents to reach the targeted region. Such breaking force can be provided by increasing the blood flow simply by fully deflating the balloon catheter for instance. But as the agents navigate deeper in the vasculature passed several branching vessels, the effect of modulating the blood blow from such a device located in the artery will be diminished. Although the gradient field is constant throughout the body, the size of the aggregate decreases due to smaller vessel's diameters when operating deeper in the vascular network, and hence the force induced becomes smaller as well. These comments only show the complexity involved and the need to tune and to characterize such nanorobotic agents as well as developing accurate models to predict the behaviors within specific physiological conditions and environments.

Magnetic pulling actuation is known to be the most effective method for navigation in the arterial network and possibly in the arterioles as well, but becomes ineffective in narrower vessels such as the capillaries. As such, torque-based magnetic actuation with nanorobotic agents in the form of artificial micro-swimmers (Dreyfus et al. 2005) including but not limited to artificial bacterial flagella (ABF) (Zhang et al. 2009b); and magnetically guided self-propelled nanorobotic agents such as magnetotactic bacteria (MTB) (Martel et al. 2009b, 2013b), provide complementary actuation methods to reach a target being accessible beyond the arterioles. Since such complementary methods are much less effective than magnetic pulling-based actuation in the arterial network, torque-based actuated and self-propelled nanorobotic agents must be injected in the vicinity of the target in the interstitial spaces and/or the microvasculature; or for intra-arterial injections, they should be encapsulated in larger magnetic pulling-based nanorobotic agents acting as carriers prior to be released closer to the microvascular network (Martel et al. 2009a).

A torque-based actuated nanorobotic agent can be made of a biodegradable polymer with embedded MNP. The characteristics of these MNP should be similar to the ones used for the pulling-based nanorobotic agents and should maintain their superparamagnetic property. Although the magnetic field required for moving a torque-based agent is typically much less than a pulling-based agent, a rotational magnetic field is required in the case of artificial micro-swimmers such as ABF, preventing the implementation of a field's strength as high as the ones being used for MRN when conceived for whole body medical interventions. This means that for whole body interventions, such embedded MNP would typically be well below the saturation magnetization value due to the limit in the magnetic field strength of the directionally controlled gradients of approximately 0.1 T. This fact must be taken into consideration for the intervention and the design of such artificial nanorobotic agents.

For magnetically guided self-propelled nanorobotic agents, this is not an issue because the magnetic torque is used for directional control or guidance only. In MTB (Blakemore 1975), a chain of intracellular single magnetic domain Fe_3O_4 nanoparticles known as magnetosomes (Bazylinski et al. 1988; Faivre and Schüler 2008) can be used to guide such flagellated bacteria acting as nanorobotic agents (Martel et al. 2009a; Martel 2013a). The level of magnetotactic directional guidance toward a physiological target region is characterized by the alignment of the cell in the applied directional magnetic field, and it is determined by the ratio of the interactive magnetic energy with the applied field to the thermal energy being the thermal forces associated with Brownian motion. Previous experiments showed that a directional magnetic field slightly higher than the geomagnetic field would be sufficient to guide such bacteria toward a pre-determined target such as a tumor in the case of drug delivery in cancer therapy. These chains of magnetosomes provide insights that could potentially lead to the exploitation of similar chain of single domain MNP in other nanorobotic agents.

Imaging

Imaging is an essential part of medical nanorobotics. Besides the imaging of the physiological environment including potential vascular routes and the localization of target sites for the nanorobotic agents, being able to image to assess the position of the nanorobotic agents in the human body is highly desirable for nanorobotic

medical interventions. Assessing the position of the nanorobotic agents can be classified as real-time and non-real-time. Real-time positioning also referred to as real-time tracking of the nanorobotic agents is typically done during the navigation phase where feedback positioning data are used to compute and apply corrective actions in order to maintain the nanorobotic agents along a planned physiological path leading to the target site. Non-real-time localization is typically used to assess the targeting efficacy of the nanorobotic agents following the navigation phase. In the latter case, the use of a relatively long acquisition time to improve detection remains an option unlike for real-time tracking.

Known medical imaging modalities include computed X-ray tomography (CT), optical imaging, magnetic resonance imaging (MRI), positron emission tomography (PET), single-photon-emission computed tomography (SPECT), and ultrasound. Among all these imaging modalities, MRI is particularly suited in acquiring 3D anatomical images in tissue samples such as human soft tissues where nanorobotic agents typically operate. This can be done with high spatial and temporal resolution. In addition, MR-images are acquired without the use of ionizing radiation such as in X-ray and CT, or radiotracers as for PET and SPECT. Furthermore, in the context of medical nanorobotics, the magnetic environment provided by a clinical MRI scanner is particularly suited as discussed earlier for the navigation of nanorobotic agents in the arterial network and the arterioles by bringing the embedded MNP at saturation magnetization for optimizing the induction of 3D gradient forces on the agents.

But another important fact is that MRI can prove to be much superior to other medical imaging modalities such as X-ray in tracking the position of nanorobotic agents. Indeed, magnetically saturated MNP embedded in nanorobotic agents operating in the B_0 field of a clinical MRI scanner produce a substantial locally perturbing dipolar field which leads to a marked shortening of the transverse (spin–spin) relaxation times T_2*. Such local dipolar field can be made sufficiently large to allow MRI to detect nanorobotic agents that have overall dimensions smaller than the spatial resolution of any clinical imaging platforms. Indeed, empirical observations suggest that an iron oxide particle disrupts the magnetic field enough for MRI detectability for a distance at least 50 times its size (Shapiro et al. 2004). In the case of iron oxide contrast agents, considering the size of a voxel at $\sim$ 500 μm for a 3T clinical MRI scanner suggests that Micrometer-sized Iron Oxide (MIO) particles instead of Ultra small Superparamagnetic Iron Oxide (USPION) particles ($<$ 50 nm) or SPION particles ($>$ 50 nm) would be preferable. Although MNP such as USPION or SPION particles are desirable for their integration in nanorobotic agents because of their superparamagnetic property allowing for clinical target interventions, a significant quantity of such MNP must be embedded in each micrometer-sized nanorobotic agent to yield significant signal changes to be detectable by MRI. Increasing the quantity of MNP in each agent up to the limit of the synthesis process also increases the induction volume but it may also reduce the payload if it is embedded within the biodegradable matrix as for the TMMC mentioned earlier. One the other hand, if such a payload can be distributed and attached to the MNP, then the payload can potentially be increased by taking advantage of the larger surface to volume ratio of MNP. But this would require that the MNP has the right characteristics for proper delivery (e.g., cell uptakes) while adding a layer that may change the properties of the MNP to maintain its suitability in the context of medical nanorobotics.

Medical nanorobotic agents generally consist of a cluster of monodispersed SD MNP embedded with a payload encased in a biocompatible material where the overall size of the agent will typically be in the micrometer range. Such microscale agent will generally cause a geometrical distortion and echo shifting in MR-images. As opposed to spin echo (SE), such echo shifting results in a signal loss in gradient echo (GE) imaging due to intravoxel dephasing. Such susceptibility-based signal loss then provides a mean to detect magnetic MNP-based microscale agents with an overall volume largely inferior to the spatial resolution of a clinical MRI scanner.

The detection threshold in MRI is a complex problem that is affected by a number of factors, including field strength, SNR, pulse sequence, and acquisition parameters (particularly the resolution and echo time (TE)) (Bowen et al. 2002), as well as the MNP loading in the nanorobotic agents and the saturation magnetization level of the MNP. Indeed, reaching a higher saturation magnetization level for the MNP not only leads to higher induced pulling

magnetic forces for the nanorobotic agents but also increases the detectability by MRI. For instance, although an image acquisition time of a few minutes was necessary, just a few TMMC agents mentioned earlier and which were based on FeCo MNP were sufficient to allow detection and localization by a 1.5T clinical MRI when in the lobe of liver of rabbit models.

The same holds true for an aggregation of nanorobotic agents. Indeed, such an aggregation not only increases the effective induction volume to yield higher actuation forces but also creates a larger MRI artifact that can be more easily detected. This is particularly important when real-time constraints during navigation must be met otherwise, the blood flow must be further reduced (or stopped for a longer period of time) which would increase the time of the intervention unless modifications of the navigation control algorithms would be done accordingly. Such modifications could take various forms such as relying on less feedback positional information and on more predictive models that would prove to be effective up to a certain limit. Such limit would typically depend on the accuracy of the theoretical models used and the level of predictability of the disturbing forces that could bring such agents away from the planned path.

Hyperthermia

One of the critical challenges in medical nanorobotics is to embed more functionality in agents that are extremely small. Embedding more functionality would lead to more advanced and more sophisticated nanorobotic agents capable of executing more complex tasks, which is a requirement for several medical interventions. In larger robots, increasing the number of functionalities is typically accomplished by adding components (hardware) or by adding such additional functions in embedded software. Since the latter is not presently possible at the scale of such nanorobotic agents, the former appears to be the only option available. But embedding additional components without increasing the overall size of each nanorobotic agent beyond an acceptable volume becomes extremely challenging. As such, one strategy is to make the embedded components multifunctional by tailoring their characteristics appropriately.

This is the case of the MNP embedded in pulling-based nanorobotic agents for instance where the same MNP are used for allowing the induction of a directional pulling force, as well as for real-time MR-tracking, MR-imaging to assess targeting efficacy, and possibly in intracellular delivery of chemotherapeutic molecules when such MNP are functionalized appropriately. But the range of functions supported by the same MNP can be expanded further, and magnetic hyperthermia being also referred to as AC hyperthermia is one additional important embedded function that is often critical for specific target nanorobotic interventions.

In cancer therapy, for example, magnetic hyperthermia is generally defined as a treatment in which higher temperatures (e.g., $\sim$ 43–46 °C for hyperthermia alone, and $\sim$ 40–43 °C when combined with chemotherapy and/or radiotherapy) are applied to kill cancer cells since the latter have proven to be more sensitive to high temperatures than healthy cells (Mornet et al. 2004). As for delivering drug molecules, achieving better targeting through medical nanorobotics would yield better treatment outcomes by magnetic hyperthermia. Such target hyperthermia could be combined with other forms of therapy including chemotherapy and radiotherapy to yield more effective treatments. Indeed, since at higher temperatures, cancer cells become more vulnerable and respond better to chemotherapeutic drugs or radiation suggest the possible implementations of more effective nanorobotic agents capable of combining two or more treatment modalities.

For superparamagnetic MNP with a magnetic volume V, an external AC magnetic field energy can force the magnetic moment to rotate and overcome the energy barrier $E = K\,V$, where K is defined as the anisotropy constant. Once the MNP relaxes to its equilibrium orientation, this energy is then dissipated in the form of heat. This mechanism is well known as the Néel relaxation. Besides Néel relaxation, Brownian relaxation can also produce heat if the MNP are free to rotate. For Brownian relaxation, the energy barrier for reorientation of a single domain MNP is provided by rotational friction due to the rotation of the entire MNP caused by the AC magnetic field torque force on the magnetic moment of the MNP. In all cases, the power of which the magnetic material is heated per gram is given by the specific absorption rate (SAR).

Besides the alternating (AC) magnetic field amplitude (H) at a given frequency (f), SAR depends also on

the nanoparticles' properties such as mean size, saturation magnetization (M_S), and magnetic anisotropy (K). An approach to increase the heat generation is the use of single domain MNP displaying hysteresis losses (Lacroix et al. 2009) which may represent a good alternative especially to compensate for a reduction of the SAR by superparamagnetic MNP designed to be immobilized into cancer cells after being released from the nanorobotic agents. In this particular case of intracellular hyperthermia, the mean size of iron oxide particles would typically be above the superparamagnetic limit of $\geq$ 15 nm and below the optimal size of $\leq$ 50 nm for internalization into mammalian cells (Zhang et al. 2009a). In typical applications, independent randomly oriented uniaxial single domain MNP will lead to a losses scaling approximately with $M_S H_C$ according to the Stoner-Wohlfarth model, where H_C represents their coercive field. Hence, metallic iron-based MNP instead of iron oxide MNP would be better in this respect due to their higher saturation magnetization. This is also in full agreement with the requirement for enhancing the induction of magnetic gradient force on a medical nanorobotic agent suggesting that the same MNP would be optimized for both purposes as well as for MR-tracking and MR-imaging. But again, the low chemical stability at physiological conditions and adequate biocompatibility are drawbacks of metallic MNP that forces the combinatory use of complex core–shell architectures (Martinez-Boubeta et al. 2010; Meffre et al. 2012).

The tuning of the magneto-crystalline anisotropy K by controlling the overall shape of the MNP can also influence the magnetic heating efficiency in MNP (Lee et al. 2011). For instance, the highest specific losses have been achieved with cubic iron MNP (Mehdaoui B. et al. 2011). Such cubic iron MNP had an effective anisotropy constant $K_{eff} = 9.1 \times 10^4$ J/m^3, and $M_S = 1.7 \times 10^6$ A/m. But to take advantage of such characteristics, the applied AC magnetic field amplitude must be sufficiently high to ensure the remagnetization of the MNP. In such a case, a SAR of approximately 3000 W/g can be achieved with a field $\mu_0 H_{max} = 73$ mT at $f = 274$ kHz. Besides achieving a high SAR for hyperthermia and high saturation magnetization for magnetic induction during gradient-based navigation, cubic MNP are also very good for MR-imaging (Lee et al. 2012).

But one critical issue is the determination of the optimal overall size for such multifunctional MNP designed to be embedded in medical nanorobotic agents. Such optimal size should be in the range of 15–50 nm for the reasons mentioned earlier. Previous studies have already reported dependence of the SAR on the mean size of cubic MNP with significant optimal SAR. For instance, 19 nm iron oxide cubic MNP have achieved optimal SAR values in clinical conditions up to 2452 W/g$_{Fe}$ at 520 kHz and 29kAm^{-1} (Guarda et al. 2012). Compared to 20 nm spherical iron oxide MNP, 20 nm cubic iron oxide MNP showed a SAR being 20 % superior under the same experimental conditions (Martinex-Boubeta et al. (2013).

For the distributed configuration of these MNP, it is important to know that dipolar coupling between MNP significantly affects the magnetic susceptibility and hysteresis losses, thus implying a considerable reduction in specific heating power for hyperthermia applications (Serantes et al. 2010; Branquinho et al. 2013). This is in agreement with the impact of the demagnetization factor of chain-like MNP structures on the hysteresis loop as well as the increase in remanence and coercivity as mentioned earlier. These facts suggest the need of coating such MNP with a thermally conductive surfactant for each MNP embedded inside the medical nanorobotic agents. Although the aggregation of biodegradable nanorobotic agents is not typically an issue, aggregation of the embedded MNP due to remanence after the biodegradation process of the medical nanorobotic agents may prove to be problematic in a clinical point-of-view unless the nanorobotic agents can be recovered, which is typically not the case in such target medical interventions. If one wants to reduce the demagnetization factor in medical nanorobotic agents, a method should be implemented to be able to demagnetize the MNP within acceptable physiological safety constraints following the navigation phase of the nanorobotic agents.

MNP in clinical nanorobotic interventions

For experiments conducted in animal models that do not involve hyperthermia, MD FeCo MNP embedded in each nanorobotic agent will provide the highest saturation magnetization and the best real-time MR-

tracking performance. But for clinical interventions conducted in humans, superparamagnetic MNP as mentioned earlier must typically be embedded in each agent with the highest emu/g per volume ratio occurring in the 6–20 nm particle size range (Jun et al. 2005). In such clinical applications, Fe_3O_4 would be more easily accepted than FeCo.

Clinical nanorobotic interventions can cover applications beyond the direct target delivery of therapeutics. For instance, besides target magnetic hyperthermia, the SAR of the embedded MNP can be exploited to allow the overall dimension of thermo-sensitive hydrogel-based medical nanorobotic agents to vary from a computer command. Such external command is used to initiate the AC magnetic field responsible for the increase in temperature of the ideal case of monodispersed MNP embedded in each hydrogel-based nanorobotic agent. Such a variation in the overall dimension of the nanorobotic agent can take the form of an increase or a decrease in the overall volume of the agent. For example, for the first proposed hydrogel nanorobotic agent (Tabatabaei et al. 2011), superparamagnetic Fe_3O_4 MNP were embedded in a biocompatible thermo-sensitive hydrogel (poly(*N*-isopropylacrylamide) - PNIPA). These spherical PNIPA-MNP nanorobotic agents were not only adequate for MRN by providing the required characteristics to allow the induction of sufficient directional pulling forces while allowing MR-tracking, but also resulted in a 25 % volume reduction of the agent when the polydispersed embedded MNP (diameters ranging from 3 to 18 nm due the unavailability of a narrower diameter range of commercial MNP) were exposed to an AC field of 4 kA/m at 160 kHz. During a medical intervention, such shrinking of the nanorobotic agents can be used for several applications such as computer-triggered drug releases or to perform a temporary embolization at a specific site in the vascular network, to name but only two examples.

If magnetic hyperthermia must be supported by the same medical nanorobotic agents, then $\sim$ 20 nm cubic (or other anisotropic shaped) Fe_3O_4 MNP should be embedded for best SAR while maintaining the highest emu/g per volume ratio. The $\sim$ 20 nm magnetic core of each MNP should be coated ideally with a thermally conductive layer or a layer allowing effective heat transfer with a thickness sufficient to minimize dipolar interactions. The total diameter of the MNP referred to as the hydrodynamic particle diameter (magnetic core + coating layer) must also be kept sufficiently small while preventing dipolar interactions in order to allow the integration of the required quantity of MNP per nanorobotic agent.

The same MNP used for MR-navigation, MR-tracking, and local hyperthermia in a medical nanorobotic agent can also be used to persuade the diffusion of therapeutic molecules across the blood brain barrier (BBB) (Tabatabaei et al. 2012). Indeed, it was observed that an elevation of the temperature of a few degrees leads to a reversible (after approx. 2 h) opening of the BBB. The main advantage of using a nanorobotic approach compared to all other methods is that the elevation of the temperature is not only done where the payload (therapeutic or diagnostic molecules) is located since both the MNP and the payload are encased in the same nanorobotic agent, but also at the cellular level therefore minimizing acute side effects due to overheating of other physiological tissues.

Although target imaging and diagnosis are other potential medical applications. Combining diagnostics with therapeutics is also possible with the use of nanorobotic theranostic agents. Although multimodal imaging could be implemented, such approach would yield more complex agents or MNP in most cases. Since such applications of nanorobotic agents typically occur in a clinical MRI environment requiring highly sensitive MR-imaging, one of the key characteristics of the MNP embedded in the nanorobotic agents is the relaxivities. In general, the relaxivities are determined, but not limited, by three key aspects of the MNP. Such aspects are the chemical composition of the MNP, the size of the MNP or construct and the degree of their aggregation if used, and the surface properties that can vary by modification and functionalization.

The chemical composition has been addressed earlier showing the gained advantage of metallic and in particular FeCo MNP over Fe_3O_4 MNP to increase the relaxivities despite the stability and potential biocompatibility issues.

About the size of the magnetic core in MNP, since M_S increases with the size of the magnetic core in the MNP, the capability of MRI signal enhancement by the MNP correlates directly with the size of the magnetic core of the MNP. But for the many reasons mentioned earlier, such size would typically be restricted to a magnetic core diameter of $\sim$ 20 nm. Another approach to improve relaxivities and hence the detection sensitivity by MRI would be the

formation of nano-clusters made of several MNP embedded in each nanorobotic agent. This could be done keeping in mind the potential negative effects of the dipolar interactions between MNP for nanorobotic target medical interventions.

Such dipolar interaction can be avoided by the use of a coating with a sufficient thickness around the magnetic core in each MNP. But the MNP shell (coating) thickness can have a significant impact on their relaxivities by compromising the efficiency of the MNP in relaxing the surrounding water molecules. As such, surface properties on the MNP can be exploited to enhance MRI contrast. Indeed, since the interactions between water and the magnetic core of each nanoparticle occur primarily on the surface of the nanoparticle, suggests that hydrophilic surface coating can be used to enhance MRI contrast effects (Duan et al. 2008). In this later study, it was confirmed that proton relaxivities of iron oxide nanoparticles coated with a copolymer depend on the surface hydrophilicity and coating thickness in addition to the coordination chemistry of inner capping ligands and the particle size. In other words, a MNP coating which facilitates the accessibility of water to the magnetic core will lead to the rapid exchange and diffusion of water molecules between the bulk phase and the adjacent layer surrounding the particle surface, yielding higher MRI contrast effects. But for metallic MNP, such approach may cause oxidation and the release of metallic ions. A thin (few nanometers) protective layer such as graphite or other materials (as mentioned earlier) that would prevent direct contact with water and oxygen can be synthesized between the magnetic core and the hydrophilic coating if the later proved to not adequately prevent such negative effects.

When MR-imaging is performed once, such MNP synthesized for MRI contrast enhancement and functionalized for a particular specificity to cancer cells, for example, are released from the nanorobotic agents, and then the issue for detectability is mostly concerned with a sufficient concentration of MNP in a particular physiological region. On the other hand, if MR-imaging or the detection of such MRI contrast-enhanced MNP must be done when they are still embedded in the nanorobotic agents, then relaxivities may be affected by the type of media inside the nanorobotic agents if not water. As such, care must be taken in the development of nanorobotic agents capable of high MRI relaxivities.

Figure 5 provides an example of a medical nanorobotic agent in the form of a schematic that summarizes the basic requirements of the embedded MNP to allow MRN, MR-tracking and imaging, as well as local hyperthermia. Although the results of many studies suggest that the MNP should be monodispersed in the nanorobotic agent as depicted in Fig. 5, another recent study (Serantes et al. 2014) suggests the formation of chain of MNP with morphology similar to the magnetosomes of magnetotactic bacteria to enhance the SAR value. The study mentions that the area of hysteresis loop increases (and therefore the SAR) with the length of the chain (observable results up to approx. 8 MNP). This behavior could be interpreted in terms of the effective anisotropy of the MNP arising from their preferential orientation along the chain due to dipolar coupling which could result to SAR values several times larger than the intrinsic SAR of an isolated particle. On the other hand, disorientation of the assembly would lead to a considerable decrease in the hysteresis loop area and to drastic effect on magnetically triggered heating. This simple example shows that much research and therefore knowledge are needed to better understand the phenomena at the nanoscale. This is critical since such better understanding would inevitably lead to more optimal design of medical nanorobotic agents.

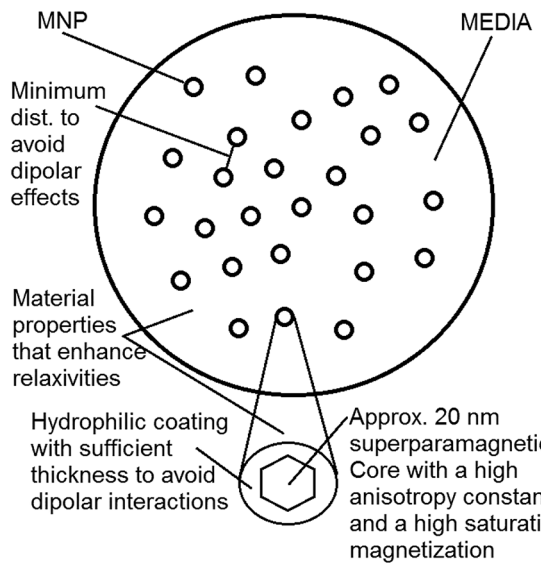

Fig. 5 Simple standard architecture of a MRN-compatible medical nanorobotic agent suited for MR-tracking and local hyperthermia. Other configurations are possible

Conclusion

The MNP used in medical nanorobotics generally share the same requirements and challenges encountered in nano-medical applications. As such, the field of medical nanorobotics benefices greatly from the results and findings obtained in nano-medicine. But in the form of nanorobotic agents, such MNP must often support additional characteristics such as enhancement of the induction of pulling gradient forces and real-time MR-tracking, to name but only two fundamental requirements that are often of strategic importance to achieve enhanced targeting efficacy. Increasing the multifunctional aspect of such MNP embedded in such nanorobotic agents is also an area of increasing importance that must be implemented within technological and physiological constraints. To date, MNP have shown to be one promising components that could fulfill such expectations and needs. Although this paper provides an idea of what MNP can achieve in medical nanorobotic agents, much needs to be done and further research is needed to push further the exploitation of MNP in the field of medical nanorobotics.

References

Bazylinski DA, Frankel RB, Jannasch HW (1988) Anaerobic magnetite production by a marine, magnetotactic bacterium. Nature 334:518–519

Belharet K, Folio D, Ferreira A (2013) Simulation and planning of a magnetically actuated microrobot navigating in the arteries. IEEE Trans Biomed Eng 60(4):994–1001

Blakemore RP (1975) Magnetotactic bacteria. Science 190: 377–379

Bowen CV, Zhang X, Saab G, Gareau PJ, Rutt BK (2002) Application of the static dephasing regime theory to superparamagnetic iron-oxide loaded cells. Magn Reson Med 48:52–61

Branquinho LC et al (2013) Effect of magnetic dipolar interactions on nanoparticle heating efficiency: implications for cancer hyperthermia. Sci. Rep. 3:2887

Dreyfus R, Baudry J, Roper ML, Fermigier M, Stone HA, Bibette J (2005) Microscopic artificial swimmers. Nature 437:862–865

Duan H, Kuang M, Wang X, Wang YA, Mao H, Nie S (2008) Reexamining the effects of particle size and surface chemistry on the magnetic properties of iron oxide nanocrystals: new insights into spin disorder and proton relaxivity. J Phys Chem C 112:8127–8131

Faivre D, Schüler D (2008) Magnetotactic bacteria and magnetosomes. Chem Rev 108:4875–4898

Guarda P et al (2012) Water-soluble iron oxide nanocubes with high values of specific absorption rate for cancer cell hyperthermia treatment. ACS Nano 6:3080–3091

Gupta AK, Gupta M (2005) Synthesis and surface engineering of iron oxide nanoparticles for biomedical applications. Biomaterials 26:3995–4021

Hergt R, Dutz S, Röder M (2008) Effects of size distribution on hysteresis losses of magnetic nanoparticles for hyperthermia. J Phys: Condens Matter 20(38):385214

Jun YW et al (2005) Nanoscale size effect of magnetic nanocrystals and their utilization for cancer diagnostic via magnetic resonance imaging. J Am Chem Soc 127(16): 5732–5733

Lacroix L-M et al (2009) Magnetic hyperthermia in single-domain monodisperse FeCo nanoparticles: evidences for Stoner-Wohlfarth behavior and large losses. J Appl Phys 105:023911

Lee JH et al (2011) Exchange-coupled magnetic nanoparticles for efficient heat induction. Nat Nanotech. 6:418

Lee N et al (2012) Water-dispersible ferrimagnetic iron oxide nanocubes with extremely high r2 relaxivity for highly sensitive in vovo MRI in tumors. Nano Lett 12:3127–3131

Martel S (2013a) Bacterial microsystems and microrobots. Biomed Microdevices 14(6):1033–1045

Martel S (2013b) Navigation control of micro-agents in the vascular network: challenges and strategies for endovascular magnetic navigation control of microscale drug delivery carriers. IEEE Cont Syst 33(6):119–134

Martel S (2014) Magnetic therapeutic delivery using navigable agents. Ther Deliv 5:189–204

Martel S, Mathieu J-B, Felfoul O, Chanu A, Aboussouan É, Tamaz S, Pouponneau P, Beaudoin G, Soulez G, Yahia L'H, Mankiewicz M (2007) Automatic navigation of an untethered device in the artery of a living animal using a conventional clinical magnetic resonance imaging system. Appl Phys Lett 90:114105

Martel S, Mohammadi M, Felfoul O, Lu Z, Pouponneau P (2009a) Flagellated magnetotactic bacteria as controlled MRI-trackable propulsion and steering systems for medical nanorobots operating in the human microvasculature. Int. J Robot Res (IJRR) 28(4):571–582

Martel S, Felfoul O, Mathieu J-B, Chanu A, Tamaz S, Mohammadi M, Mankiewicz M, Tabatabaei N (2009b) MRI-based nanorobotic platform for the control of magnetic nanoparticles and flagellated bacteria for target interventions in human capillaries. Int. J Robot Res (IJRR) 28(9):1169–1182

Martinex-Boubeta C et al (2013) Learning from nature to improve the heat generation of iron-oxide nanoparticles for magnetic hyperthermia applications. Sci. Rep. 3:1652

Martinez-Boubeta C et al (2010) Self-assembled Fe/MgO nanospheres for magnetic resonance imaging and hyperthermia. Nanomed. Nanotech. Biol. Med. 6:362–370

Mathieu J-B, Martel S (2009) Aggregation of magnetic microparticles in the context of targeted therapies actuated by a magnetic resonance imaging system. J. Appl Phys. 106:1–044904

Mathieu J-B, Beaudoin G, Martel S (2006) Method of propulsion of a ferromagnetic core in the cardiovascular system through magnetic gradients generated by an MRI system. IEEE Trans Biomed Eng 53(2):292–299

Meffre A et al (2012) A simple chemical route toward monodisperse iron carbide nanoparticles displaying tunable magnetic and unprecedented hyperthermia properties. Nano Lett 12:4722–4728

Mornet S, Vasseur S, Grasset F, Duguet E (2004) Magnetic nanoparticle design for medical diagnosis and therapy. J Mater Chem 14(14):2161–2175

Ngo A-T, Pileni M-P (2000) Nanoparticles of cobalt ferrite: influence of the applied field on the organization of the nanocrystals on a substrate and on their magnetic properties. Adv Mater 12(4):276–279

Pouponneau P, Leroux J-C, Soulez G, Gaboury L, Martel S (2011) Co-encapsulation of magnetic nanoparticles and doxorubicin into biodegradable microcarriers for deep tissue targeting by vascular MRI navigation. Biomaterials 32(13):3481–3486

Pouponneau P, Segura V, Savadogo O, Lweroux J-C, Martel S (2012) Annealing of magnetic nanoparticles for their encapsulation into microcarriers guided by vascular magnetic resonance navigation. J Nanopart Res 14:1307–1320

Pouponneau P, Bringout G, Martel S (2014) Therapeutic magnetic microcarriers guided by magnetic resonance navigation for enhanced liver chemoembolization: a design review". Ann Biomed Eng 42(5):929–939

Reiss G, Hutten A (2005) Magnetic nanoparticles–Applications beyond data storage. Nat Mater 4:725–726

Serantes et al (2010) Influence of dipolar interactions on hyperthermia properties of ferromagnetic particles. J Appl Phys 108:073918

Serantes et al (2014) Multiplying magnetic hyperthermia response by nanoparticle assembling. J Phys Chem C 118:5927–5934

Shapiro EM, Skrtic S, Sharer K, Hill JM, Dunbar CE, Koretsky AP (2004) MRI detection of single particles for cellular imaging. PNAS 101(30):10901–10906

Tabatabaei SN, Lapointe J, Martel S (2011) Shrinkable hydrogel-based magnetic microrobots for interventions in the vascular network. Adv. Robot 25:1049–1067

Tabatabaei SN, Duchemin S, Girouard H, Martel S (2012) Towards MR-navigable nanorobotic carriers for drug delivery into the brain, IEEE Conf. Robot Autom 14:727–732

Voltairas PA, Fotiadis DI, Michalis LK (2002) Hydrodynamics of magnetic drug targeting. J Biomech 35:813–821

Zhang L, Abbott JJ, Dong L, Peyer KE, Kratochvil BE, Zhang H, Bergeles C, Nelson BJ (2009a) Characterizing the swimming properties of artificial bacterial flagella. Nano Lett 9(10):3663–3667

Zhang S, Li J, Lykotrafitis G, Bao G, Suresh S (2009b) Size-dependent endocytosis of nanoparticles. Adv. Matter. 21:419